



Characterization of the density-driven counter-flow through a doorway using Large Eddy Simulation

Elyas Larkermani^{*}, Guangyu Cao, Laurent Georges

Norwegian University of Science and Technology, Department of Energy and Process Engineering, Kolbjørn Hejes v 1B, NO-7491, Trondheim, Norway

ARTICLE INFO

Keywords:

Natural convection
Large vertical opening
Discharge coefficient
Large eddy simulation

ABSTRACT

The density-driven bidirectional flow through an open doorway is of prime importance for ventilation and heat distribution between rooms in buildings. Although this flow has been extensively studied in the past, some important flow characteristics, such as unsteady flow phenomena, have not been documented in detail. Therefore, a high-resolution Large Eddy Simulation (LES) of the bulk flow through a doorway is performed. This LES can also serve as a reference solution to compare the accuracy of simpler evaluation methods, from the standard theoretical model calibrated using a discharge coefficient (C_d) to CFD solving the Reynolds-Averaged Navier-Stokes (RANS) equations. Based on LES results, the bidirectional flow can generate turbulent mixing in the middle of the doorway. However, the effects remain limited to the close vicinity of the neutral plane. The bidirectional airstream in the doorway further develops into two non-isothermal jets that entrain a fraction of the airflow. Furthermore, the two jets create large unsteady flow structures when they expand in the adjoining rooms. The results show that unsteady RANS is a good alternative to the resource-intensive LES if the analysis of turbulent jets is not of interest. The standard theoretical model demonstrates that two-dimensional contraction is the dominant effect driving the C_d value, while the viscous effects have a minor influence. Unlike previous studies, LES results show that viscous effects tend to increase the C_d as they moderate the contraction effect. This paper also provides guidelines for the laboratory measurement of C_d and its use in building performance simulation tools.

1. Introduction

Natural convection in confined spaces has received considerable interest due to its prominent role in ventilation, air conditioning and indoor air contaminants transmission. In most situations, heat and mass are convected through an opening located within an internal partition wall between two enclosures by an intrinsically three-dimensional and transient flow field. The characteristics of such a complicated flow are of great importance to many applications and practical research fields. Specifically, airflow through large vertical openings could significantly contribute to the thermal behavior of buildings and the air circulation patterns in a room [1]. The influence of airflow is also determinant in transmitting airborne diseases, such as COVID-19. For instance, the airflow through large openings could be vital in hospital operating theatres where the passage of airborne diseases to clean rooms increases the risk of infection [2–6]. Hence correct estimation of doorway flow rates and flow patterns is essential from the airborne contaminant control point of view.

1.1. Flow regimes

Several mechanisms, such as pressure and density differences, occupant movement, and door motion, may drive the airflow through a large vertical opening [7]. A combination of different mechanisms along with many physical parameters makes it complex to derive a general solution for a counter-flow passing through an opening. However, it is important to distinguish between the *boundary layer flow* and *bulk flow* regimes. In the boundary layer flow regime, the air temperature inside an interconnected multizone enclosure is almost equal everywhere, while the temperature difference between the air and the walls generates boundary layers that drive the flow along the walls of the room. In this case, no significant difference in hydrostatic pressure arises between two adjoining rooms. In the bulk flow regime, the temperature difference between the room air and its walls is limited, which corresponds to the isothermality factor close to unity. In this regime, the air temperature difference between interconnected rooms leads to a difference in hydrostatic pressure that drives the flow through the door opening. A

^{*} Corresponding author. Kolbjørn Hejes v 1B, NO-7491, Trondheim, Norway.
E-mail address: elyas.larkermani@ntnu.no (E. Larkermani).

previous study by Allard et al., IEA EBC Annex 20 [8], demonstrated that the bulk flow regime is dominant in buildings.

The transition from the boundary layer to the bulk flow regime was examined in the experimental studies of Scott et al. [9] and Neymark et al. [10]. This transition between both flow regimes was explained by the blockage effect when the aperture size in the partition wall starts to be small. Georges et al. [11] conducted Computational Fluid Dynamics (CFD) simulations of a bidirectional flow through a doorway using the Reynolds-Averaged Navier-Stokes (RANS) approach. Unlike the previous works of Scott et al. [9] and Neymark et al. [10] that neglect thermal radiation between walls, Georges et al. [11] showed that, in addition to the aperture size, the thermal radiation strongly influences the isothermality factor and thus the flow regime.

1.2. Standard theoretical model

In Building Performance Simulation (BPS) tools like TRNSYS or IDA ICE [12], the volume of air in each thermal zone is isothermal. Airflow networks, such as COMIS [13] or CONTAM [14], are used to compute the airflows between the interconnected zones [15]. The standard (or conventional) model assumes a bulk flow to compute airflow rates through large vertical openings in airflow networks. It considers two isothermal reservoirs at different temperatures and a one-dimensional inviscid steady-state flow. These assumptions lead to a simple model based on the Bernoulli equation, defined here as the standard theoretical model [8].

The resulting maximum theoretical flow is then corrected using the discharge coefficient (C_d) to match the actual airflow in the doorway. The C_d can be calibrated on the actual mass ($C_{d,M}$) or the heat flow ($C_{d,Q}$). Allard and Utsumi [16] mentioned that this phenomenological coefficient includes the effect of local flow contraction caused by the vertical opening (i.e., a two-dimensional effect). They investigated various approaches to determine the C_d , which may be expressed as a function of opening height or the air temperature difference between the interconnected rooms. They demonstrated the difficulty of determining the C_d and pointed out that various definitions for this coefficient have been introduced in the literature. They concluded that the definition of C_d is still ambiguous and requires more precise simulation or experimental measurements. Heiselberg et al. [17] argued that the different values of C_d for door openings reported in previous studies might be attributed to simple and unrealistic assumptions. The uniform air temperature distribution inside the enclosures and the one-dimensional flow field at the opening are clear examples of these assumptions.

1.3. Knowledge gap

The bulk flow through a doorway has been investigated extensively, for instance, in IEA EBC Annex 20 [8]. However, several characteristics of the flow have not been studied in detail.

Assuming an inviscid flow, the velocity profile shows a sharp

gradient at the level of the neutral plane (NP), see Fig. 1(a). With viscous flow, two related phenomena shown in Fig. 1(b) can occur in the vicinity of the NP:

- The two airstreams going in opposite directions create a shear layer. In a recent study by Lefaue et al. [18], two reservoirs filled with a fluid of different densities were connected by a long channel. They demonstrated that a sustained stratified shear flow could generate large unsteady flow structures.
- Wilson and Kiel [19] reported some interfacial mixing between the two airstreams in opposite directions. Interfacial mixing causes a fraction of the warm airflow initially flowing towards the opening to be brought back into the warm zone, entrained by the cold airstream. This re-entrainment effect also takes place for the cold airflow and leads to an exchange of momentum between the two counter-flowing streams passing through a large vertical opening. According to these authors, the resulting velocity and temperature profiles are smoother at the level of the NP compared to inviscid flow, as shown in Fig. 1(a). Consequently, the mass and heat flow exchanged through the doorway could be reduced compared to the inviscid flow (i.e., the assumption used in the standard model).

Detached shear layers are formed at the edges of the doorway. According to the literature review, the transition of these detached shear layers into a three-dimensional turbulent flow has not been investigated in earlier studies. The two airstreams in the opposite direction develop non-isothermal jets in the adjoining rooms, which is a phenomenon that has scarcely been documented in the literature. Finally, most existing studies report on the velocity field, and a few of them analyzed the temperature field within the doorway in detail. However, the temperature field directly impacts the convective heat transfer between interconnected rooms. The main objective of this paper is to characterize flow separation at the opening edge, interfacial mixing between counter-flowing streams and turbulent flow development.

1.4. Need for high-resolution CFD

To answer this question, the bulk flow passing through a doorway between a warm and a cold room can be investigated using laboratory measurements or CFD. Several previous studies have measured the airflow characteristics between two chambers at different temperatures separated by a partition wall, e.g. Refs. [8,20,21]. They typically relied on intrusive flow measurements using low-velocity anemometers. These measurements are demanding since they should be done at many locations within the aperture of the doorway and inside both rooms due to the three-dimensional nature of the airflow field. As it will be shown in the paper, measuring the airflow only along a vertical line in the middle of the doorway leads to rough simplifications. Consequently, the airflow should be measured in the entire doorway, which is demanding. Moreover, anemometers have a lower accuracy for air velocity magnitudes

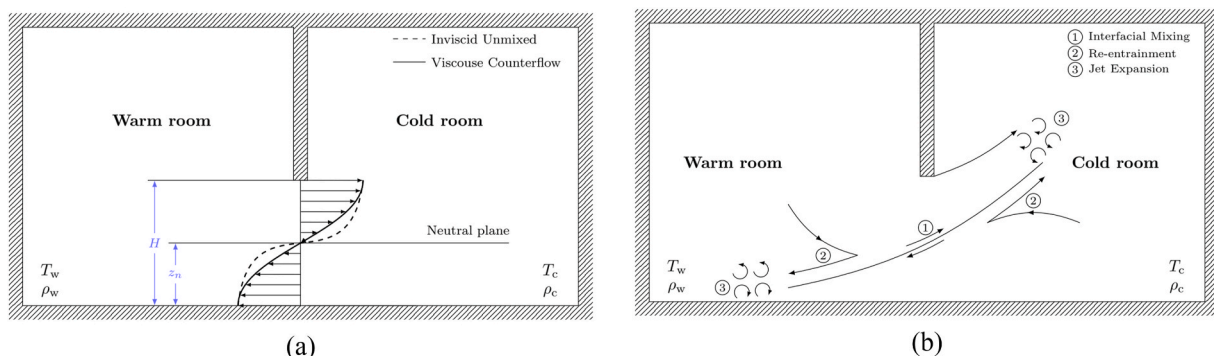


Fig. 1. Streamwise velocity profiles (left) and re-entrainment by cross-stream interfacial mixing (right) for the bidirectional flow in a doorway.

below 0.1 m/s, which are typically found in the middle of the doorway. Non-intrusive measurement methods such as Particle Image Velocimetry (PIV) are also demanding as the flow needs to be visualized over several meters, the typical door height (H) being 2 m. However, a common methodology for investigating airflows in buildings uses non-dimensional analysis and water on reduced-scale models [9,22]. This makes the use of PIV easier. However, the effect of thermal radiation would not be addressed using water [10,22,23], and the flow regime would most likely not be a density-driven bulk flow. Finally, tracer gases or smoke visualization can be used [5], but they do not measure physical quantities, like velocity, locally in the doorway. In conclusion, laboratory measurements are possible but challenging to investigate the physical phenomena introduced in Section 1.3.

Several studies have investigated the bulk flow through large vertical openings using CFD. However, these studies are not appropriate to address the physical phenomena explained in Section 1.3. Firstly, these studies did not aim to capture these complex unsteady flow phenomena. As an example, Favaro and Manz [24] used the LVEL $k-\epsilon$ turbulence model [25] in the FloVENT commercial CFD software. They analyzed the impact of different parameters, such as the temperature difference between indoor and outdoor air and the location of large openings on the C_d . Secondly, these studies were conducted using unsteady RANS turbulence modeling. It has not been proven that the RANS approach is appropriate to capture the instabilities of the shear flows for this particular case.

Large Eddy Simulation (LES) has the potential to provide more reliable and detailed information about the natural ventilation in buildings on a sufficiently fine grid resolution [26–30]. The large-scale structures of indoor airflows containing most of the energy are explicitly resolved using LES, while small scales that tend to be more isotropic and universal are filtered out. LES is more appropriate than RANS to capture the flow instabilities this paper seeks to characterize. LES of the flow through a doorway has been performed in the past but on relatively coarse meshes compared to the computational power that is currently available, see, e.g. Ref. [31]. A previous study by Saarinen et al. [5] investigated the flow through a doorway using LES with a high resolution, but they considered the transient regime when the door between both rooms is suddenly opened, and an occupant moves through the door.

1.5. Research questions

Consequently, high-resolution LES of the bulk flow passing through the doorway in a steady-state regime is performed using the Wall-Adapting Local Eddy-viscosity (WALE) subgrid scale model in ANSYS Fluent. The geometry and boundary conditions are developed to approximate a single laboratory experiment with significant temperature stratification in the warm and cold rooms, the baseline case. Measurements and CFD results are compared for this test case.

As explained in Section 1.3, the main research question is to characterize flow separation at the opening edge, interfacial mixing between counter-flowing streams and turbulent flow development (Q1). However, with this reference solution (i.e., high-resolution LES), complementary research questions can also be addressed:

- Viscous effects can be distinguished from two- and three-dimensional effects by comparing Euler (i.e., inviscid solution) to RANS and LES solutions (Q2).
- The ability of the RANS method to capture the bulk flow can be investigated by comparing it to the reference LES solution (Q3).
- The influence of temperature stratification in both rooms can be investigated by comparing the LES solutions of the baseline case with temperature stratified rooms with the second case of two isothermal interconnected rooms at different temperatures (Q4).
- As BPS software typically assumes isothermal rooms, the error created by neglecting stratification can be discussed (Q5).

- The influence of the measurement setup on the evaluation of C_d can be clarified. For instance, the mass and heat flow can be measured in the entire doorway plane or along a single vertical line in the middle of the doorway to reduce the number of measurement points (Q6).

2. The standard theoretical model of bulk flow

The air temperature difference (ΔT) between warm and cold zones in an interconnected multizone enclosure and the aperture geometry are the only physical parameters needed to define the bulk flow regime. In this case, the room air temperature is assumed to be in thermal equilibrium with the wall temperature. The air temperature difference between both sides of the opening leads to different air densities and, consequently, different hydrostatic pressure fields. Due to the conservation of mass, hydrostatic pressure fields on both sides of the opening are equal at the NP located near the middle of the doorway, see Fig. 1(a). The difference in hydrostatic pressure above and below the NP generates two counter-flowing streams of warm and cold air. The standard model equations are derived for two interconnected isothermal reservoirs in Section 2.1, while the difference compared to thermally stratified rooms is explained qualitatively (i.e., without the model equations).

2.1. Airflow between two interconnected isothermal rooms

Assuming inviscid and steady flow, the problem can be solved by applying the Bernoulli equation between two points along a streamline passing from one semi-infinite reservoir to another. With a one-dimensional flow field assumption, the Bernoulli equation can be written in the following way along a horizontal streamline that connects a point located in the warm room to a point close to the opening but in the cold room:

$$p_w(z) + \rho_w g z = p_D(z) + \rho_w g z + \rho_w \frac{u_D(z)^2}{2} \quad (1)$$

where subscripts W and C indicate the warm and cold rooms, respectively, while subscript D refers to the level of the doorway. z denotes the vertical distance from the floor. The pressure of the flow entering the receiving room (p_D) is assumed to be equal to the hydrostatic pressure in that room, i.e. $p_D(z) = p_C(z)$. As both rooms are isothermal with negligible velocity, the integration of the hydrostatic equation along z enables the static pressures p_w and p_C to be related to the floor pressure for the warm and cold rooms, respectively:

$$p_w(z) = p_w(0) - \rho_w g z \quad (2)$$

$$p_C(z) = p_C(0) - \rho_C g z \quad (3)$$

Substituting expressions (2) and (3) in Equation (1) gives the vertical profile of the horizontal velocity through the door opening from the warm room to the cold room:

$$u_{wC}(z) = \sqrt{\frac{2}{\rho_w} (p_w(0) - p_C(0) - (\rho_w - \rho_C) g z)} \quad (4)$$

The level of the NP (z_N) can be computed directly by imposing $u_{wC}(z_N) = 0$:

$$z_N = \frac{p_w(0) - p_C(0)}{(\rho_w - \rho_C) g} \quad (5)$$

Using the definition of the NP in Equation (4) removes the need to evaluate the pressure difference between the rooms at the floor level. The theoretical velocity profile above the NP from the warm room to the cold one is then defined as:

$$u_{wC}(z) = \sqrt{\frac{2g(\rho_C - \rho_w)}{\rho_w} (z - z_N)} \quad z \geq z_N \quad (6)$$

By following the same procedure along a streamline connecting a particle moving from the cold to the warm room, one obtains:

$$u_{CW}(z) = \sqrt{\frac{2g(\rho_C - \rho_W)}{\rho_C}}(z_N - z) \quad z \leq z_N \quad (7)$$

A schematic representation of these two velocity profiles for bidirectional flow along the doorway is depicted in Fig. 1(a).

The corresponding maximum theoretical mass flow rate per unit width above and below the NP is given by:

$$\dot{m}_{WC}(z) = \int_{z_N}^H \rho_W u_{WC}(z) dz = \frac{2}{3} \rho_W \sqrt{\frac{2g(\rho_C - \rho_W)}{\rho_W}} (H - z_N)^{3/2} \quad (8)$$

$$\dot{m}_{CW}(z) = \int_0^{z_N} \rho_C u_{CW}(z) dz = \frac{2}{3} \rho_C \sqrt{\frac{2g(\rho_C - \rho_W)}{\rho_C}} z_N^{3/2} \quad (9)$$

The sum of these two mass flow rates must respect the conservation of mass. In other words, the mass flow entering the sealing room must equal the mass flow leaving the room ($\dot{m}_{WC}(z) = \dot{m}_{CW}(z) = \dot{m}_{\max}(z)$). This mathematical constraint enables the neutral layer location to be expressed as a function of air densities:

$$z_N = \frac{H}{\left(1 + \left(\frac{\rho_C}{\rho_W}\right)^{1/3}\right)} \quad (10)$$

indicating warm airstream above the NP is thicker than the cold airstream below the NP as $\rho_W < \rho_C$.

In reality, the flow is neither inviscid nor one-dimensional. The airflow has contraction and viscous effects. Therefore, the actual mass flow rate is obtained by applying a correction factor, the discharge coefficient ($C_{d,M}$), to the maximum theoretical mass flow rates from Equations (8) and (9):

$$\dot{m}_{\text{actual}} = C_{d,M} \dot{m}_{\max} \quad (11)$$

For sharp-edged openings, $C_{d,M}$ is about 0.6 [19].

A convective heat transfer between two interconnected zones is generated by the density-driven airflow. Assuming a constant specific heat capacity (c_p), the theoretical net heat flow rate convected per unit width is given by:

$$\begin{aligned} \dot{Q}_{\max} &= \int_{z_N}^H \rho_W u_{WC}(z) c_p (T_W - T_{\text{ref}}) dz - \int_0^{z_N} \rho_C u_{CW}(z) c_p (T_C - T_{\text{ref}}) dz = \int_{z_N}^H \rho_W u_{WC}(z) c_p T_W dz - \int_0^{z_N} \rho_C u_{CW}(z) c_p T_C dz = c_p (T_W \dot{m}_{WC}(z) - T_C \dot{m}_{CW}(z)) \\ &= \dot{m}_{\max} c_p (T_W - T_C) \end{aligned} \quad (12)$$

where T_{ref} is the reference temperature that can be eliminated due to the conservation of mass. With a uniform room air temperature, the actual heat flow rate is a fraction of the theoretical net heat flow rate:

$$\dot{Q}_{\text{actual}} = \dot{m}_{\text{actual}} c_p (T_W - T_C) = C_{d,M} \dot{m}_{\max} c_p (T_W - T_C) = C_{d,M} \dot{Q}_{\max} = C_{d,Q} \dot{Q}_{\max} \quad (13)$$

According to the standard theory, this proves that the same $C_{d,i}$ (i.e., $C_{d,M} = C_{d,Q}$) can be used for both mass and heat flow rates when both rooms are isothermal.

2.2. Airflow between two interconnected stratified rooms

In Section 2.1, the air temperature was assumed to be uniform in both rooms. However, in reality, the air temperature is often not isothermal within a room, an important effect being the vertical

temperature stratification. This stratification impacts the vertical profile of hydrostatic pressure and thus the location of the NP [7]. Moreover, unlike isothermal rooms, the velocity profiles are no longer parabolic in the aperture.

In most applications, the vertical air temperature distribution can be assumed to be linear [32–34]. The equations of the standard models in Section 2.1 can be extended for a case with linear vertical temperature stratification [7]. In this case, the most important conclusion is the prediction of a same discharge coefficient for the mass and heat flows by the standard theoretical model, as for the isothermal rooms.

3. Methodology

3.1. Experimental setup

The experiment has been conducted by Paul Minard [35] in a full-scale climate chamber. The environmental chamber consists of two rooms connected by an open doorway of height 1.9 m and width 0.83 m located in the middle of the vertical partition wall. The dimensions of the warm and cold rooms are $2.65 \times 2.3 \times 3.8 \text{ m}^3$ and $3.9 \times 7.8 \times 6.9 \text{ m}^3$ ($H \times W \times D$), respectively. The partition wall has a thickness of 0.1 m. Both rooms are equipped with a mechanical ventilation system that is turned off during the experiment. Two electric panel heaters were installed in the warm room far away from the door while the cold room was not heated. Ten omnidirectional anemometers TSI 8475 (with accuracy $\pm 3\% \pm 0.005 \text{ m/s}$) and PT-100 sensors (with accuracy $\pm 0.1^\circ\text{C}$) were mounted on a vertical bar located in the middle of the doorway to measure air velocity and temperature. The sensors were uniformly distributed along z from the floor to the top of the door. The surface of all PT-100 sensors is coated with aluminum to limit the effect of thermal radiation. The temperature stratification inside the warm and cold rooms was measured with five PT-100 sensors mounted on a vertical pole, 2 m away from the opening. When radiators were turned on, it took several hours before steady-state conditions were reached. Then, data were recorded every 20 s during a period of 10 min. More details about the procedure and probe locations can be found in Refs. [11,35].

3.2. Computational domain

Measurements showed significant temperature stratification in both

rooms, especially in the heated room. It is challenging to reproduce the same stratification in CFD. It would require detailed measurements of the surface temperature for both rooms and the heat emitters. Fortunately, measurements revealed that the airflow was in the bulk flow regime. Consequently, the computational domain was defined to enforce this bulk flow regime rather than to reproduce the exact geometry of the laboratory. In this respect, the rooms were defined considerably larger than the doorway size (Fig. 2). In addition, the measured temperature stratification is imposed as initial conditions within both reservoirs. At the start of the simulation, when both reservoirs are put in contact, a transient flow is established through the doorway until it reaches a pseudo steady-state. The same procedure was followed in the experimental setup of Lefauve et al. [18]. As both rooms are large, the convective heat transfer through the doorway does not have time to significantly influence the temperature of both reservoirs during the period of physical time computed by the CFD. The partition wall has the

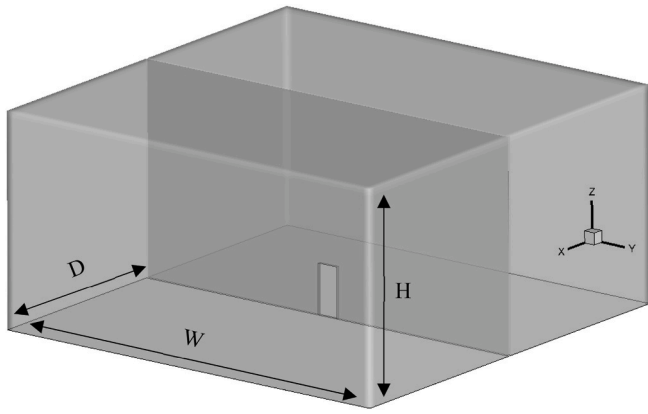


Fig. 2. Three-dimensional multizone enclosure configuration ($H \times W \times D = 8 \times 16 \times 8 \text{ m}^3$).

same thickness as the laboratory experiments.

3.3. Governing equations

Applying an implicit filtering operator and considering the Boussinesq approximation in the body force term, the filtered incompressible Navier-Stokes equations solved by the LES can be expressed as:

$$\frac{\partial \bar{u}_i}{\partial x_i} = 0 \quad (14)$$

$$\frac{\partial \bar{u}_i}{\partial t} + \frac{\partial \bar{u}_i \bar{u}_j}{\partial x_j} = -\frac{1}{\rho_{\text{ref}}} \frac{\partial \bar{p}}{\partial x_i} + \frac{\partial}{\partial x_j} [2\nu \bar{S}_{ij}] - \frac{\partial \tau_{ij}}{\partial x_j} + g_i [1 - \beta(\bar{T} - T_{\text{ref}})] \quad (15)$$

$$\frac{\partial \bar{T}}{\partial t} + \frac{\partial \bar{u}_j \bar{T}}{\partial x_j} = \frac{\partial}{\partial x_j} \left[\alpha \frac{\partial \bar{T}}{\partial x_j} \right] - \frac{\partial \tau_{jT}}{\partial x_j} \quad (16)$$

where the bar represents the implicit grid filtering, x_i denotes the i^{th} spatial coordinate direction, \bar{u}_i represents the filtered velocity field in the x_i direction, t the time, \bar{p} the modified filtered pressure, and \bar{T} the filtered temperature. The last term in Equation (15) is the buoyancy term where $\beta = 1/T_{\text{ref}}$ is the thermal expansion coefficient of the air modeled as an ideal gas and g_i the gravitational acceleration. The parameters ν and α indicate the kinematic viscosity and thermal diffusivity, respectively. They are assumed constant (i.e., independent of the air temperature) and taken for the air at T_{ref} . The subgrid scale (SGS) stress tensor and the scalar SGS thermal flux vector are included, respectively, in the momentum and energy equations above via the unresolved terms $\tau_{ij} = \bar{u}_i \bar{u}_j - \bar{u}_i \bar{u}_j$ and $\tau_{jT} = \bar{u}_j \bar{T} - \bar{u}_j \bar{T}$.

3.4. SGS modeling in LES

The closure of the Navier-Stokes equations can be achieved by utilizing the WALE turbulence model to calculate the SGS kinematic viscosity, ν_{SGS} , based on the invariants of the velocity gradient tensor:

$$\tau_{ij} = \bar{u}_i \bar{u}_j - \bar{u}_i \bar{u}_j = -2\nu_{\text{SGS}} \bar{S}_{ij} + \frac{2}{3} k_{\text{SGS}} \delta_{ij} \quad (17)$$

$$\nu_{\text{SGS}} = \bar{\Delta}^2 C_w^2 \frac{(\bar{S}_{ij}^* \bar{S}_{ij}^*)^{3/2}}{(\bar{S}_{ij} \bar{S}_{ij})^{5/2} + (\bar{S}_{ij}^* \bar{S}_{ij}^*)^{5/4}} \quad (18)$$

$$\bar{S}_{ij}^* = \frac{1}{2} (\bar{g}_{ij}^2 + \bar{g}_{ji}^2) - \frac{1}{3} \bar{g}_{kk}^2 \delta_{ij} \quad (19)$$

$$\bar{g}_{ij}^2 = \bar{g}_{ik} \bar{g}_{kj} = \frac{\partial \bar{u}_i}{\partial x_k} \frac{\partial \bar{u}_k}{\partial x_j} \quad (20)$$

where C_w is the model coefficient, here taken at a constant value of 0.325 [36], and the effective filter width is computed using the local cell volume, $\bar{\Delta} = \sqrt[3]{V_k}$. k_{SGS} and \bar{S}_{ij} are the SGS kinetic energy and resolved scale strain rate tensor:

$$\bar{S}_{ij} = \frac{1}{2} \left(\frac{\partial \bar{u}_i}{\partial x_j} + \frac{\partial \bar{u}_j}{\partial x_i} \right) \quad (21)$$

By analogy to the SGS stress tensor modeling, the scalar SGS thermal flux vector, τ_{jT} , can be approximated by the following expression [37]:

$$\tau_{jT} = \bar{u}_j \bar{T} - \bar{u}_j \bar{T} = -\frac{\nu_{\text{SGS}}}{Pr_{\text{SGS}}} \frac{\partial \bar{T}}{\partial x_j} \quad (22)$$

where Pr_{SGS} denotes the SGS Prandtl number and is fixed at 0.85. The WALE SGS model has been selected for the following reasons. The WALE turbulence model is able to reproduce the near-wall behavior correctly. Thus, unlike the Smagorinsky SGS model, which requires a wall-damping function, the WALE eddy viscosity model recovers the proper y^3 near-wall scaling for the turbulent eddy viscosity [38]. The model also generates zero turbulent viscosity in the case of pure shear. Therefore, it is expected to capture the transitional flow from laminar to turbulent [38,39]. On top of that, the formulation of the WALE SGS model depends on both the strain and the rotation rate of the small turbulent structures, making WALE model a more reliable SGS model than the dynamic Smagorinsky model to predict the interfacial mixing layer accurately [38,40,41].

To investigate the influence of turbulence modeling, unsteady RANS is also employed here using the most common turbulence model for ventilation flow prediction, i.e., the RNG k- ϵ model [42]. The governing equations for this method would be the Reynolds-averaged incompressible Navier-Stokes equations.

3.5. Grid

A structured grid with 127,316,480 hexahedral cells is generated for the interconnected grid with rooms. A refined uniform grid has been defined in the vicinity of the doorway. The finest elements have a dimension of 0.6 cm to properly resolve interfacial mixing, re-entrainment, and other unsteady flow phenomena. For the sake of the conciseness, the design of the grid and the resulting LES resolution are discussed in Appendix. The aperture area on the y-z plane is covered by 44800 cells and extruded in the x-direction by 20 cells. A smooth transition between cells of different sizes is performed. The maximum growth ratio of 1.03 is adopted for top corners far enough from the doorway and 1.008 is used inside a domain of 1.5 m around the doorway. The computational grid is shown in Fig. 3.

3.6. Boundary conditions and initialization

In order to keep the temperature inside the reservoirs constant in time during the simulations, all walls including the partition wall, are assumed to be adiabatic. Slip boundary conditions are applied to each wall. This explains why no near-wall grid refinement is necessary, as no boundary layer is generated.

The bidirectional airflow through the aperture is simulated for the stratified interconnected rooms (i.e., the baseline case) and also for two isothermal rooms at different temperatures. For the baseline case, the temperature stratification measured in Paul Minard's experiments [35] is used as the initial temperature. This one-dimensional vertical air temperature profile is applied to the computational domain using User Defined Function (UDF) hooked in ANSYS Fluent. For the test case with isothermal reservoirs, no experimental data is available. Hence, the measured air temperature from the stratified case averaged along the vertical direction (z) is taken as the initial condition for the temperature. This leads to a temperature difference of 1.68 °C ($\Delta T = 1.68^\circ\text{C}$). The reference temperature (T_{ref}) is the arithmetic average of the room air

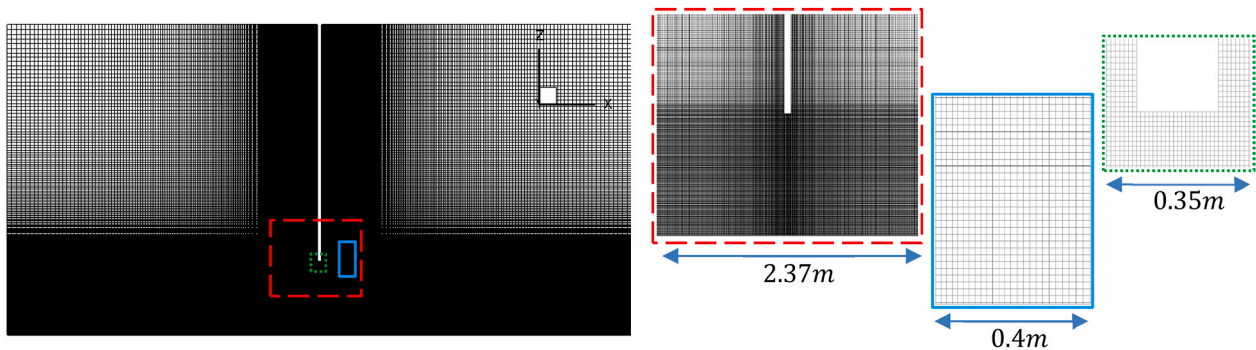


Fig. 3. Computational grid.

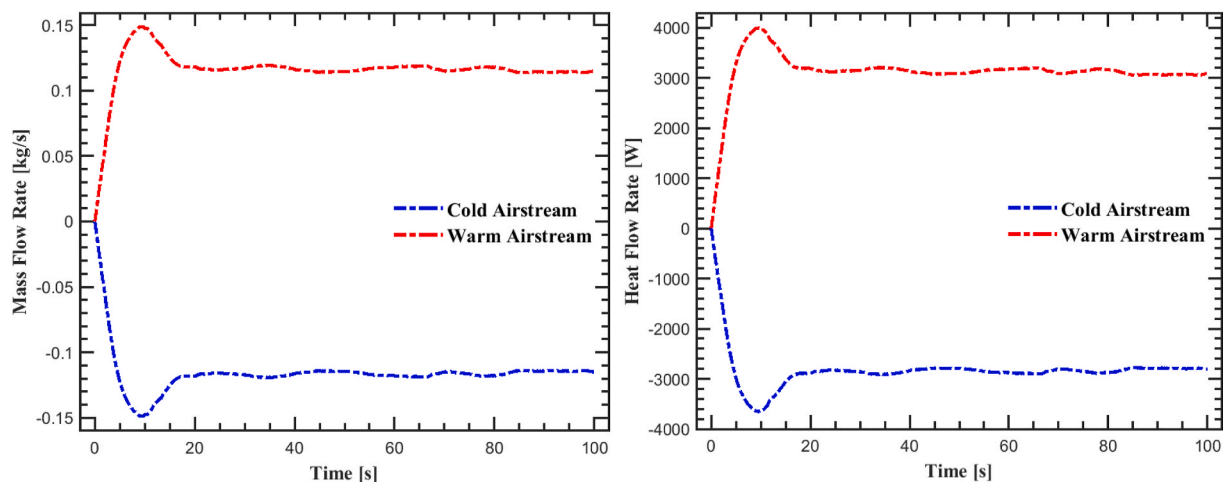


Fig. 4. Time histories of mass (left) and heat (right) flow rates for the stratified baseline case.

temperatures taken at the level of the NP in the middle of the warm and cold zones. Despite preliminary tests showing that initializing the simulation with URANS before switching to LES could partly reduce the initialization time, both enclosures are initialized with zero velocity for simplicity and to ensure that the initialization procedure does not impact the final results. As a result, each room acts as a large reservoir, and the flow through the doorway is only driven by the differences of hydrostatic pressure in both reservoirs.

During the first phase of the simulation, the bidirectional airflow passing through the doorway is strongly transient. A pseudo-stationary regime is reached after about 60 s of physical time. Then, the airflow is fully established throughout the enclosure, and the transition to turbulent flow is settled. This can be clearly seen from the time histories of heat and mass flow rates for each airstream shown in Fig. 4. In this pseudo-steady state regime ($t > 60$ s), data are collected during 40 s to reach full-converged time-averaged statistics. During this period, the volume-averaged air temperature of both reservoirs remains almost constant.

3.7. Solver settings

The nonlinear governing equations are discretized using the second-order cell-centered finite volume method (FVM) implemented in the ANSYS Fluent commercial CFD package. The *Semi-Implicit Method for Pressure Linked Equations* (SIMPLE) algorithm is employed for pressure-velocity coupling. The time derivatives are advanced in time using the *Second Order Implicit* scheme. In the LES, a constant time step of $\Delta t = 0.01$ s is applied to keep the Courant number below 1.0 to achieve high temporal accuracy. For the LES, the *Central Differencing* scheme is adopted for the treatment of the convective terms of the governing

equations, while a *Second Order Upwind* scheme is used for the RANS and Euler simulations. The pressure interpolation is provided by the *Body Force Weighted* scheme, recommended by the ANSYS Fluent User's Guide.

ANSYS Fluent is capable of running on distributed processors and uses the public domain Open MPI implementation of the standard Message Passing Interface (MPI) to conduct inter-processor communication. The present LES simulations were performed on the resources provided by UNINETT Sigma2, the National Infrastructure for High Performance Computing and Data Storage in Norway. The simulations are performed on a 15-node cluster equipped with multiple 32-core Intel Xeon processors leading to a total of 480 cores and a minimum of 160 GB of RAM.

4. Results

4.1. Description of the flow

The analysis of results starts with a general description of the flow. The instantaneous velocity magnitude field on the opening plane and midplane computed using LES is shown in Fig. 5. The time-averaged temperature field is reported in Fig. 6(a) and (b). As expected, a bidirectional flow is generated. Warm air flows from the warm room (on the left) to the cold room (on the right) in the higher part of the doorway, while the cold air flows in the opposite direction in the lower part of the doorway. Both airstreams flowing in opposite directions (i.e., bidirectional flow) generate a shear layer. The shear layer in the middle of the doorway is inclined by 39° upwards compared to the horizontal plane. This clearly indicates that the airflow through the doorway is not horizontal, as assumed by the standard theory. Moreover, both airstreams

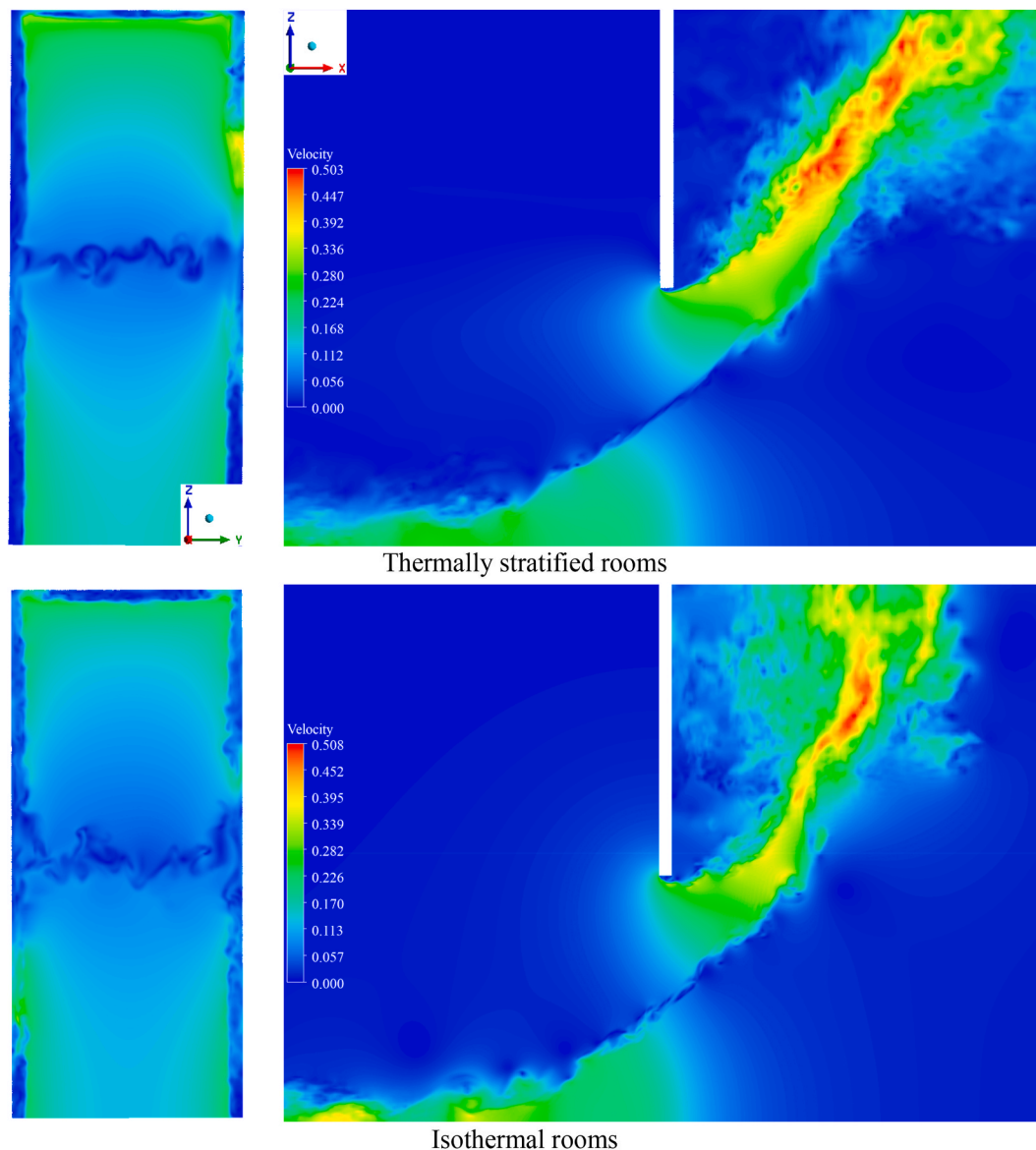


Fig. 5. Instantaneous velocity magnitude in the doorway y - z plane (left) and on an x - z plane at the middle of the door (right).

undergo a contraction when they expand in the opposite room. This contraction, known as the *vena contracta* effect, decreases the mass flow through the doorway compared to the standard theory and partly explains the need to introduce a discharge coefficient. The warm airstream develops into a warm jet that expands upwards in the cold zone, while the cold airstream develops as an attached cold jet along the floor in the warm zone. The velocity magnitude is zero near the middle of the doorway at the location of the NP.

This general description of the bidirectional airflow passing through the doorway can be deduced from all the CFD models used in this study (meaning LES, RANS and Euler), as shown in Fig. 6. Euler simulation is the only exception since inviscid flow does not generate a shear layer between the opposite airflows. Nevertheless, it is worth mentioning that the Euler equations are discretized spatially using a second-order upwind scheme that introduces some amount of artificial numerical dissipation (even though this is limited). This is enough to smooth sharp spatial gradients or generate spurious unsteadiness in the flow.

4.2. Characterization of the re-entrainment

The re-entrainment is a result of interfacial mixing between counter-

flowing streams. However, re-entrainment focuses more on the air-streams that develop into turbulent jets in the opposite rooms. Turbulent jets generate entrainment, and it should be investigated how much of the air in the opposite airstream is diverted from the doorway by this phenomenon. The streamlines in Fig. 6 show that the warm rising jet modifies the airflow direction of the cold air approaching the doorway. This effect is less pronounced for the cold jet expanding in the warm zone. Compared to RANS and Euler, re-entrainment computed by the LES deviates the airflow on a more extensive zone (highlighted by a dashed rectangle in Fig. 6), especially for the thermally stratified rooms. This shows that the re-entrainment is more important using LES and can be under-estimated using RANS.

4.3. Characterization of the shear layer mixing

The time-averaged streamwise velocity and air temperature along a vertical line in the middle of the doorway are depicted in Fig. 7. The transition between the temperature of the warm airstream and the cold airstream indicates the thickness of the shear layer. In addition, the shear layer thickness can also be assessed by the time-averaged temperature field on the midplane in Fig. 6. Analyzing the flow near the NP

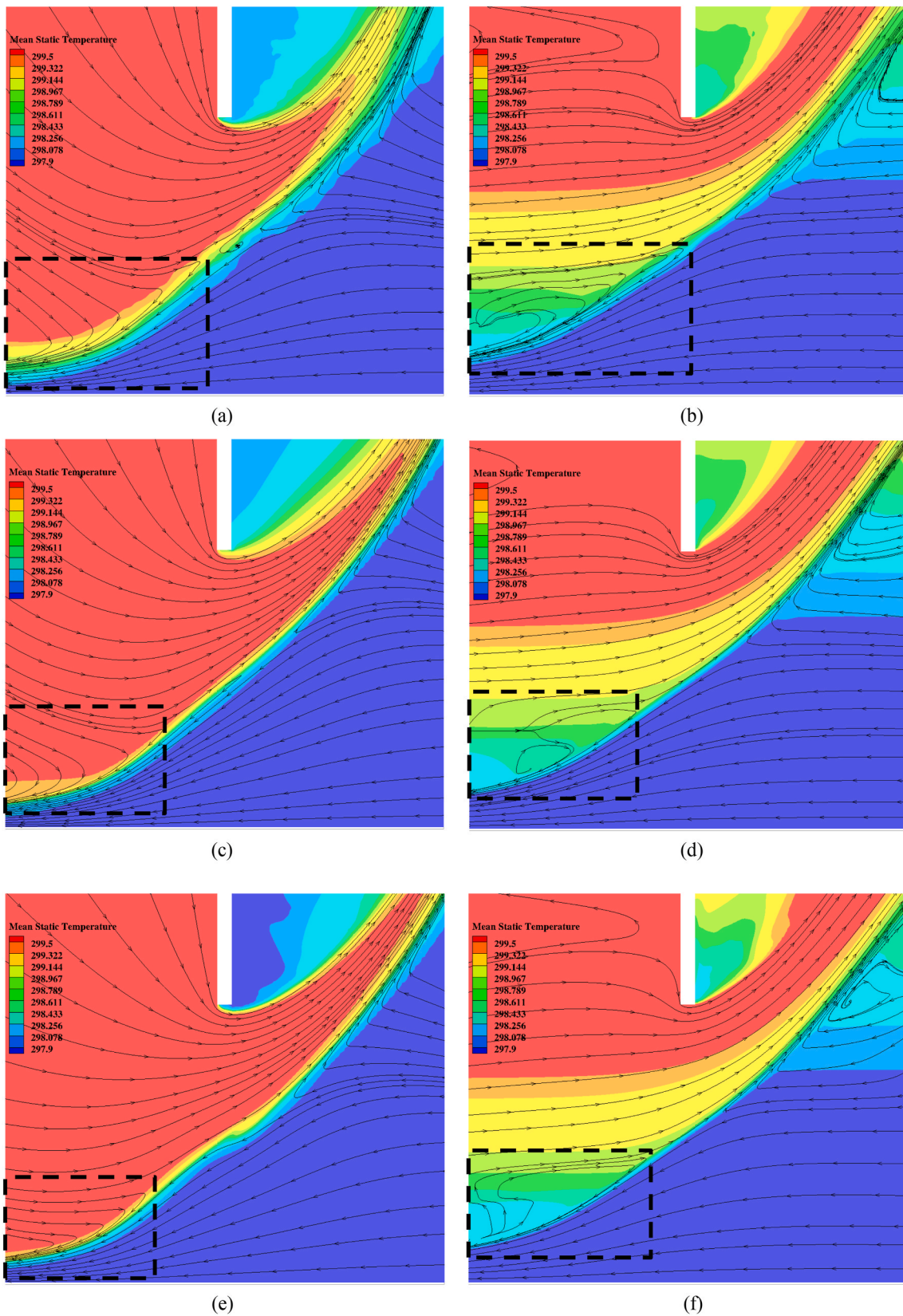


Fig. 6. Mean temperature with streamlines on the vertical plane ($y = 0$) obtained from LES (top), RANS (middle) and Euler (bottom) in isothermal rooms (left) and thermally stratified rooms (right). A dashed black box highlights a region where the re-entrainment of warm airstream occurs.

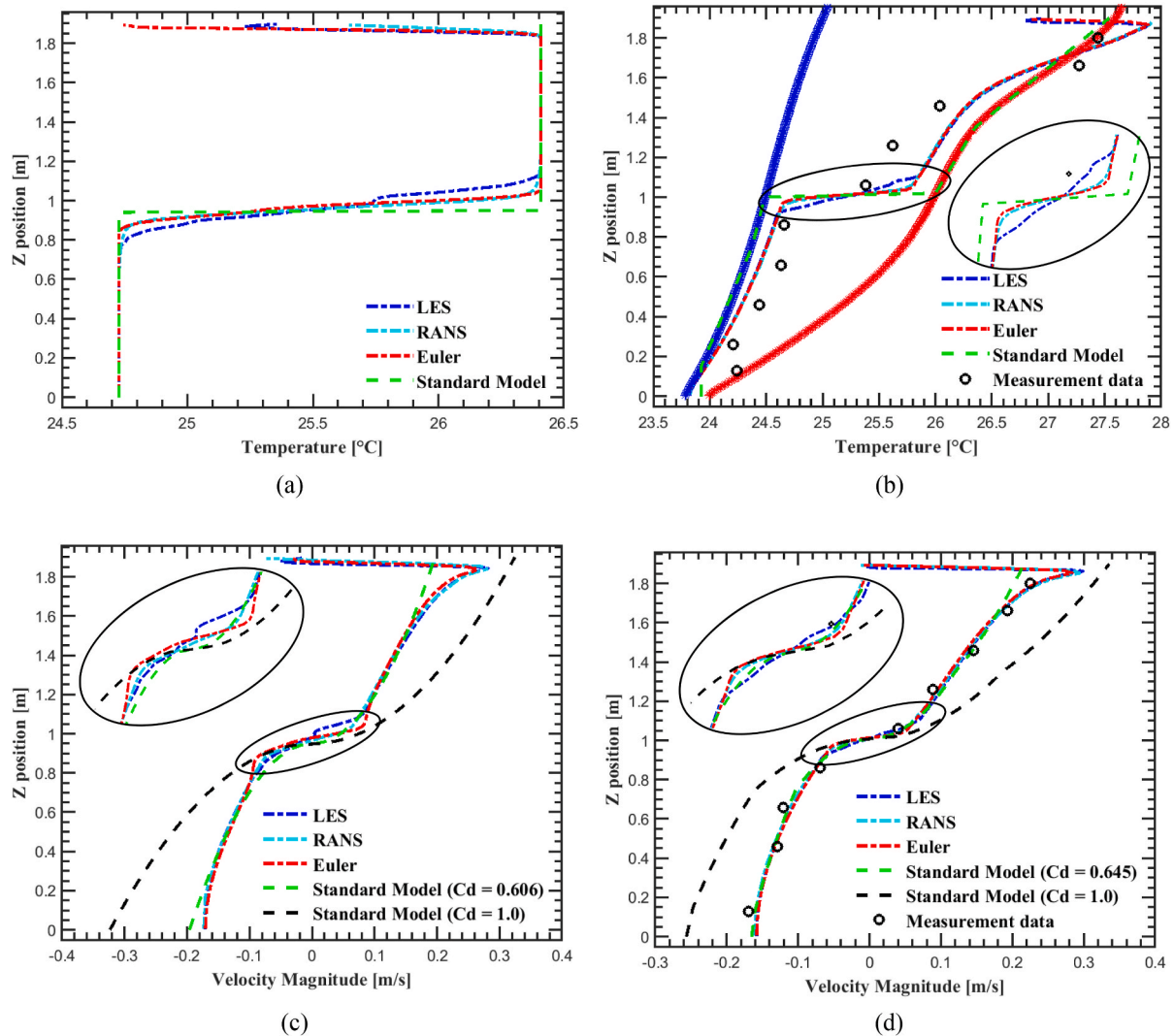


Fig. 7. Time-averaged temperature (a,b) and streamwise velocity (c,d) profiles along a vertical line in the middle of the doorway in isothermal rooms (left) and thermally stratified rooms (right). The thick blue and red lines in the thermally stratified case (b) indicate the vertical profiles of measured air temperature in the cold and warm zones, respectively. (For interpretation of the references to colour in this figure legend, the reader is referred to the Web version of this article.)

in Fig. 6 and 7 shows limited differences between the LES, RANS and Euler solutions for the baseline case with thermally stratified interconnected rooms, suggesting that the shear layer generates no intense interfacial mixing. In the isothermal interconnected rooms, the Euler and RANS are almost equal. However, the shear layer generated by the LES for this case is slightly thicker and can be explained by the mixing generated by the unsteady flow structures shown in Fig. 5. In conclusion, unsteady flow structures do not systematically develop in the middle of the doorway. If they develop, these structures and the resulting mixing remain limited in the vicinity of the NP.

4.4. Unsteady flow structures

A well-resolved LES can capture unsteady flow structures and turbulent mixing precisely. The instantaneous velocity field in Fig. 5 revealed that the flow develops several unsteady flow structures that could not be captured using unsteady RANS. The main observations are:

- The warm and cold jets become turbulent when they expand in the cold and warm rooms, respectively.

- Unsteady flow structures are generated in the shear layer near the NP between two isothermal rooms, while these structures are not visible when both rooms are thermally stratified.
- The NP is not a straight horizontal line and fluctuates in the vertical direction. These fluctuations are more pronounced in the isothermal rooms than in the thermally stratified rooms. To the authors' best knowledge, these time variations of the NP have not been reported in the literature.
- The airflow is detached at the edges of the doorway, from the horizontal head jamb but also from the vertical side jambs. The LES shows that these detached flows are unsteady, especially in isothermal rooms.

Fig. 8 depicts turbulent kinetic energy (k) contours computed using unsteady RANS and LES on the vertical midplane. While RANS does not predict any level of turbulence between counter-flowing streams along the interfacial mixing layer, the LES provides a region of lower k near the NP in the middle of the doorway, followed by a higher magnitude of k when the non-isothermal jets expand in the adjoining rooms. This can be attributed to unsteady flow structures generated in the shear layer and turbulent mixing where jet expansion occurs. LES of both isothermal and thermally stratified cases predict higher k where the detached shear

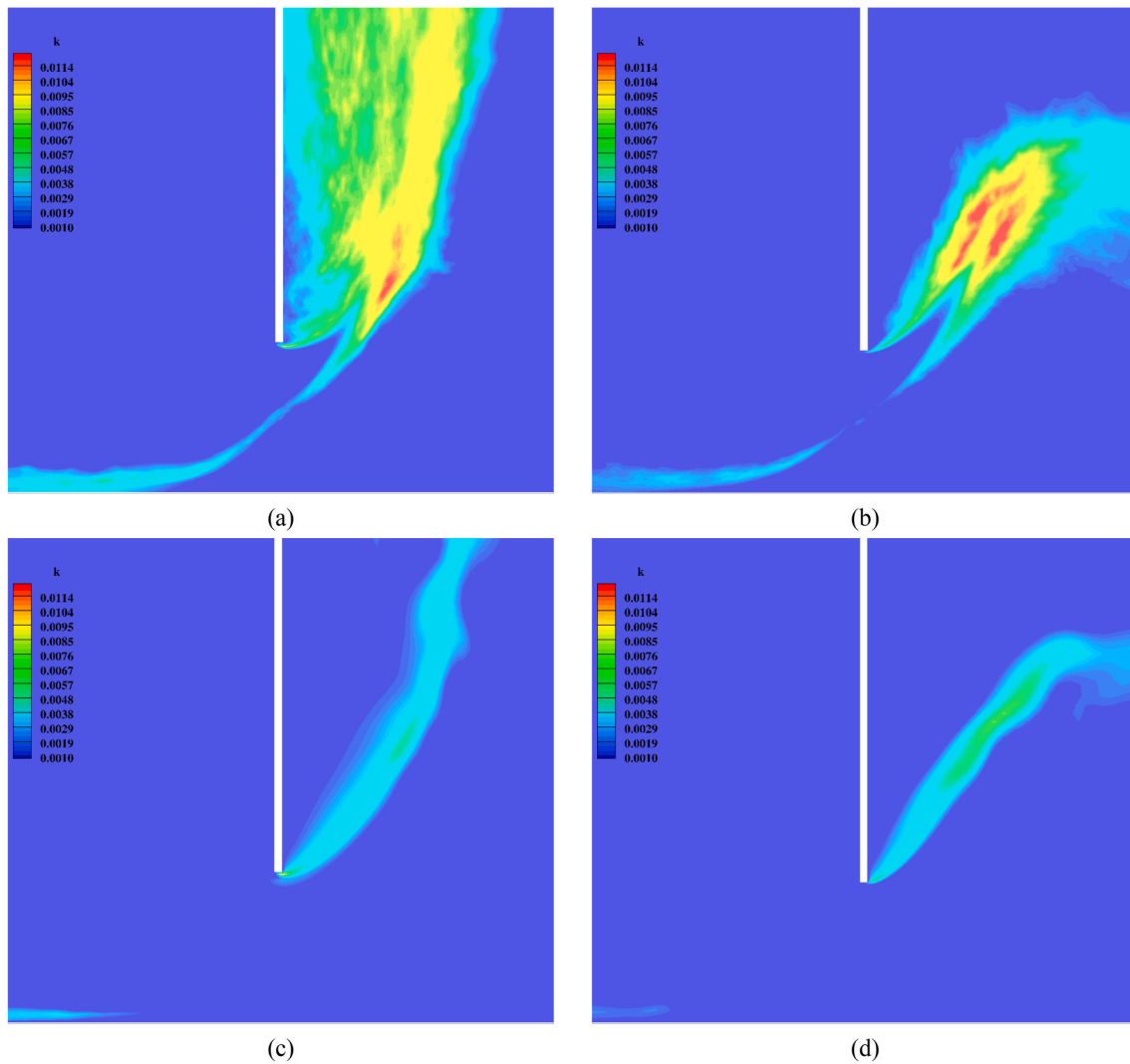


Fig. 8. Contours of turbulent kinetic energy (k) on the vertical plane ($y = 0$) obtained from LES (top) and RANS (bottom) in isothermal rooms (left) and thermally stratified rooms (right).

layer and interfacial mixing layer merge. Compared to thermally stratified rooms, the warm jet spreads in a broader area in the cold room for the isothermal case, in line with the jet expansion observed in Fig. 5, which is more extensive along the vertical partition wall. This indicates that the warm jet cannot develop up to the ceiling in the thermally stratified cold room as the temperature difference between the warm jet and cold zone disappears progressively with height.

4.5. Comparison with experiments and with the standard model

Time-averaged experimental results are reported along a vertical line in the middle of the doorway in Fig. 7(b) and (d). The time-averaged streamwise velocity in Fig. 7(d) computed using LES, RANS, and Euler shows excellent agreement with laboratory measurements with an average deviation of less than 10%. However, the measured temperature in Fig. 7(b) is only qualitatively similar to the LES, RANS and Euler results. This means that the time-averaged temperature above the NP moves progressively from the temperature of the cold zone to the temperature of the warm zone over a same distance (from the NP at about 0.9 m–1.6 m above the floor). Quantitatively, the measured and CFD simulated temperatures show a significant deviation up to 0.5°C. A plausible reason is the influence of longwave thermal radiation from the laboratory walls that could impact the sensor (PT-100) measurements. The mean radiant temperature observed by the PT100 probes is between

the wall temperature of the cold and warm rooms. It could explain that the air temperature measurements in the lower and upper part of the doorway are not strictly equal to the temperature of the cold and warm rooms, respectively. Another reason for this deviation could be the approximation of the laboratory by two large reservoirs in the CFD geometry.

In conclusion, the comparison with the experimental measurements shows reasonably good agreement with CFD results. However, on the one hand, the number of measurement points is limited, and on the other hand, the temperature field shows only similar behavior. Nevertheless, they tend to demonstrate that the same physics is investigated in both experimental and CFD conditions.

For a discharge coefficient based on the mass flow ($C_{d,M}$) computed using the LES, the standard model gives a velocity profile close to measurements, except on the top part of the doorway, where the standard model underpredicts the velocity magnitude because it neglects important 2D effects (Fig. 7(d)). The temperature profile predicted by the standard theory is defined by the one-dimensional and inviscid flow assumptions meaning that the air temperature below the NP within the doorway is equal to the temperature of the cold room, while above the NP, it is equal to the warm room temperature. In other words, the temperature transition in the standard model between the warm and cold airstreams is discontinuous. This discontinuity is located at the level of the NP that can be obtained using Equation (10). For the isothermal

rooms, the transition computed by the CFD is smoother even though limited in the close vicinity of the NP. For the stratified rooms, as mentioned in the previous section, the transition happens over a considerable vertical distance from about 0.9 m to 1.6 m above the floor. In conclusion, unlike the time-averaged velocity magnitude, the time-averaged temperature from the standard theory deviates from reality over a large fraction of the doorway.

4.6. Bulk quantities and C_d

The mass (\dot{m}) and heat flows (\dot{Q}) are analyzed either only using data along a vertical line in the middle of the doorway (like in the laboratory experiments) or using data in the entire doorway plane. The measurement setup along a vertical line in the middle of the doorway is also relevant as it is done in several studies, such as in the laboratory measurements considered in our paper [35]. It should be checked if limiting the measurement points to a single vertical line strongly impacts the bulk quantities and the C_d . Two discharge coefficients, $C_{d,M}$ and $C_{d,Q}$, are evaluated using \dot{m} or \dot{Q} , respectively. Based on the conclusions from the previous section and the values of C_d in Table 1, the following conclusions can be derived. The case using CFD data over the entire doorway plane is analyzed first as this is a consistent evaluation of the mass and heat flows:

- The discharge coefficient evaluated by the Euler model is similar to the LES and RANS values. A maximum deviation of up to 10% can be found. It means that the largest part of the C_d value can be explained by the difference between Euler and the standard theoretical model, namely the two-dimensional contraction effects.
- For the thermally stratified rooms where the interfacial mixing is limited, the difference of C_d between Euler, RANS and LES is minimal (e.g., from 0.494 to 0.509 for the $C_{d,M}$). The difference between the $C_{d,M}$ and $C_{d,Q}$ is evaluated in the last column of Table 1. This value is similar for the Euler, RANS and LES, the $C_{d,Q}$ being about 8% lower than the $C_{d,M}$.
- For the isothermal rooms where the interfacial mixing is not negligible, the difference of C_d between Euler, RANS and LES is more considerable and up to 10%. The difference between $C_{d,M}$ and $C_{d,Q}$ is

different between the Euler, RANS and LES: the $C_{d,Q}$ is 3.4% lower for Euler to 6.8% lower for the LES.

- The difference between RANS and LES is practically very small (maximum 5%).

The discharge coefficient computed using the data along a vertical line in the middle of the doorway is also reported in Table 1. In this case, the contraction effects due to the finite width (W) of the door along the vertical side jambs are neglected. Then, the resulting C_d is systematically overestimated. In addition, the difference between the $C_{d,M}$ and $C_{d,Q}$ looks more pronounced than using data over the entire door opening. This is a spurious effect that can be explained by Equation (12). According to the theory, the reference temperature (T_{ref}) can be removed from the equation because the mass is conserved. However, in reality, the flow is three-dimensional and the \dot{m}_{WC} is not strictly equal to \dot{m}_{CW} when they are evaluated along a single vertical line. Consequently, the heat flow is still dependent on the definition of T_{ref} , which is not appropriate.













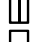
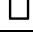
5. Discussions

Based on the analysis of the results, the research questions from Q1 to Q6 defined in the introduction section can be answered:

- Q1: The unsteady flow structures and turbulent mixing have been characterized in Section 4.
- Q2: Based on the analysis of the discharge coefficient in Section 4.6, the C_d value can be mainly explained by the two-dimensional effects, while introducing viscous effects with the RANS and LES generate a maximum change of 10%. According to Wilson and Kiel [19], the re-entrainment effect should lead to lower mass flow rates and thus C_d . However, Table 1 reveals that the C_d using Euler simulations is lower than CFD simulations including viscous effects, like RANS and LES. This result is not intuitive, but a reasonable physical explanation can be given. As previously mentioned, the flow contraction is the dominant factor driving the C_d value. Fig. 9 shows the time-averaged velocity magnitude on a plane perpendicular to the warm jet near the maximum of flow contraction. One can see that the Euler simulation leads to a more concentrated jet than RANS. As the blockage from

Table 1

Discharge coefficients obtained based on the mass ($C_{d,M}$) and heat flow rate ($C_{d,Q}$) for isothermal and thermally stratified rooms: values computed with data over the entire doorway are indicated by an empty rectangle, while values computed using data along a vertical line in the middle of the doorway are represented by a divided rectangle.

		$C_{d,M} = \frac{\dot{m}_{actual}}{\dot{m}_{max}}, C_{d,Q} = \frac{\dot{Q}_{actual}}{\dot{Q}_{max}}$		Center Line 	Doorway Plane 	$E\% = \frac{ C_{d,M} - C_{d,Q} }{C_{d,M}}$
Thermally stratified rooms	\dot{m}_{max} and \dot{Q}_{max} based on measured room temperature	LES		0.626	0.680	8.6
				0.509	0.464	8.8
		RANS		0.636	0.626	1.5
				0.509	0.468	8
		Euler		0.621	0.635	2.2
		Measurement		0.494	0.457	7.5
Isothermal rooms	\dot{m}_{max} and \dot{Q}_{max} based on the averaged room temperature	LES		0.606	0.558	7.9
				0.543	0.506	6.8
		RANS		0.619	0.699	12.92
				0.519	0.492	5.2
		Euler		0.595	0.536	9.91
				0.495	0.478	3.4

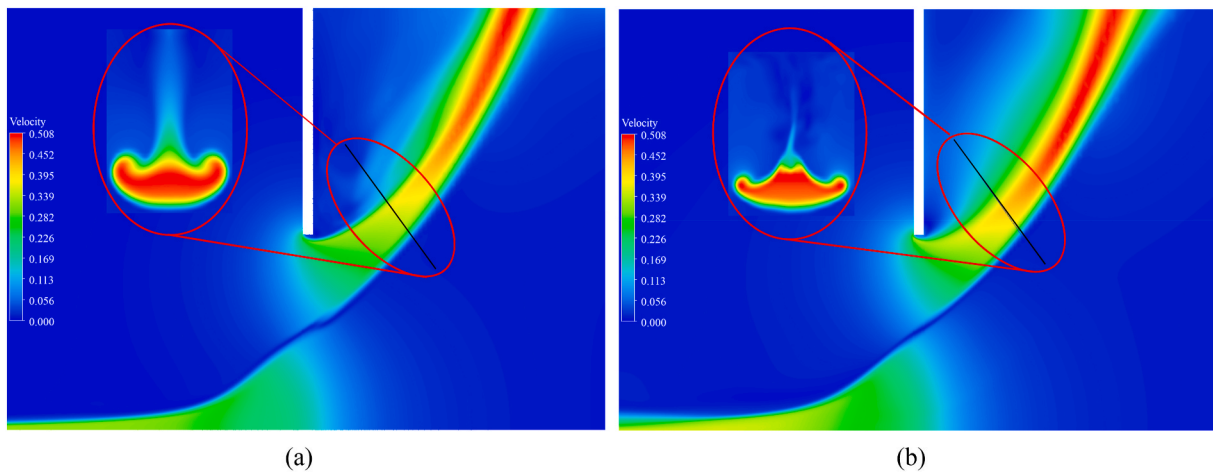


Fig. 9. Time-averaged velocity magnitude from RANS (left) and Euler (right) taken on a plane perpendicular to the jet near the maximum of flow contraction.

this contraction is more important in the Euler simulation, the C_d is lower.

- Q3: The RANS simulation using the RNG k- ϵ model gives similar results to LES. The interfacial mixing in the middle of the doorway can be underestimated by RANS simulations. However, this mixing in LES remains in the close vicinity of the NP. More importantly, RANS is not able to capture the transition of the airstreams into unsteady turbulent jets when they expand in the opposite rooms, as shown by the contours of turbulent kinetic energy in Fig. 8.
- Q4: The temperature stratification has a significant effect on the temperature distribution within the doorway due to two-dimensional effects (see Section 4.5). The transition between the temperature of the cold room below the NP and the temperature of the warm room above the NP takes place over a large part of the doorway (from 0.9 to 1.6 m). This leads to a significant deviation compared to the temperature field used in the standard theory. In addition, unsteady flow structures are less pronounced in the stratified room case than in the isothermal case. Both cases have been simulated using the exact same CFD setup. The explanation for this last phenomenon should be investigated in further research work.
- Q5: In BPS, the temperature in each room is assumed to be isothermal [43]. The mass and heat fluxes exchanged by a bidirectional airflow in the doorway are computed using the standard model corrected by a discharge coefficient, as described in Section 2.1. If the air temperature simulated by BPS in each room is precisely equal to the measured air temperature averaged along the vertical direction (z), the data in Table 2 shows that there are large discrepancies

between the resulting $C_{d,M}$ and $C_{d,Q}$ if the rooms are not isothermal in reality (up to 46%). The $C_{d,M}$ is only slightly affected when the stratification in both rooms is neglected in the standard model. However, the largest influence is on the $C_{d,Q}$ which increases significantly. Since the convective heat flux is the product of the velocity and the temperature, If the estimate of the velocity is reasonable, the temperature advected on the upper and lower parts of the doorway is respectively lower and higher in the case of isothermal reservoirs than when taking the vertical stratification into account. The maximum theoretical heat flow (\dot{Q}_{max}) is thus lower when the two rooms are assumed to be isothermal compared to the stratified rooms, leading to a higher $C_{d,Q}$. In BPS, a single C_d is typically defined to tune the mass and heat flow to the real values. If the room is stratified, the C_d should, in reality, be different for the mass and heat flows to match the reality.

- Q6: Evaluating the discharge coefficient based on measurements along a vertical line in the middle of the doorway leads to significant errors (see Section 4.6). It overestimates the $C_{d,M}$ as the contraction effects along the vertical side jambs are neglected. Mass imbalance along the vertical line makes the evaluation of the heat flow dependent on the T_{ref} , which is not reliable.

The CFD setup has been defined to reproduce the flow measurements in a climate chamber. However, the limited number of measurement points does not constitute a full experimental validation of the CFD results. Therefore, detailed laboratory measurements or additional LES should be performed in future work.

Table 2

Discharge coefficients obtained based on the mass ($C_{d,M}$) and heat flow rate ($C_{d,Q}$) for BPS analysis: values computed with data over the entire doorway are indicated by an empty rectangle, while values computed using data along a vertical line in the middle of the doorway are represented by a divided rectangle.

	$C_{d,M} = \frac{\dot{m}_{actual}}{\dot{m}_{max}}, C_{d,Q} = \frac{\dot{Q}_{actual}}{\dot{Q}_{max}}$		Center Line		$E\% = \frac{ C_{d,M} - C_{d,Q} }{C_{d,M}}$
			Doorway Plane	Doorway Plane	
Thermally stratified rooms	\dot{m}_{max} and \dot{Q}_{max} based on the averaged room temperature (for BPS analysis)	LES			74.6
					46.28
		RANS			57.99
					47.97
		Euler			64.57
					48.57
Measurement				70.76	

6. Conclusions

The airflow passing through an open doorway in the steady-state bulk flow regime was simulated using a high-resolution Large Eddy Simulation (LES), which enabled the capture of unsteady flow phenomena. In addition, this LES can serve as a reference solution for simplified methods, like Reynolds-Averaged Navier-Stokes (RANS) approaches or the standard theoretical model. The conclusions can be summarized as follows:

- The main objective of this study was to characterize the bidirectional unsteady flow phenomena. Firstly, the LES revealed that the bidirectional flow can generate a turbulent mixing region near the neutral plane (NP). However, results found that this effect remains located in the close vicinity of the NP so that its influence is limited. LES also showed that the instantaneous NP is not a horizontal line but rather fluctuating in the vertical direction. Secondly, the LES confirmed that the re-entrainment from the two non-isothermal jets expanding from the doorway deflects a fraction of the flow that would otherwise have moved towards the doorway. Finally, LES showed that the non-isothermal jets develop large unsteady flow structures when they expand in the opposite room.
- Results suggest that the RANS approach reproduces most of the flow characteristics from LES, except for the large unsteady flow structures generated by the jet expansion far away from the door. If this effect is not important in the application, RANS simulations are a good alternative to the time-consuming LES for this flow.
- The discharge coefficient (C_d) is mainly driven by two-dimensional contraction effects. Comparing Euler simulation to RANS simulation or LES revealed that viscous effects have a lower influence on the C_d than these contraction effects. Unlike previous results from the literature, the results from this study found that the viscous effects tend to increase the C_d as they decrease the flow contraction. This effect dominates over the mixing effects that tend to decrease the C_d .

The results also enabled guidelines to be derived for the evaluation and use of the C_d with the standard theoretical model:

- The C_d should not be evaluated only based on measurement along a vertical line in the middle of the doorway, as two-dimensional effects from the vertical side jambs of the doorway would be neglected. In addition, the discharge coefficient for the heat flow ($C_{d,Q}$) is inconsistent using measurements along a vertical line.
- In building performance simulation (BPS), rooms are typically modeled as isothermal reservoirs. If, in reality, the rooms are thermally stratified, a same C_d cannot be used in BPS to calibrate both the mass flow and the heat flow. Two separate discharge coefficients, i. e., $C_{d,Q}$ and $C_{d,M}$, should be defined for the BPS to compute the right mass and heat exchanges through the doorway.

CRedit authorship contribution statement

Elyas Larkermani: Writing – review & editing, Writing – original draft, Visualization, Validation, Software, Resources, Methodology, Investigation, Formal analysis, Data curation, Conceptualization. **Guangyu Cao:** Writing – review & editing, Visualization, Validation, Methodology, Conceptualization. **Laurent Georges:** Writing – review & editing, Writing – original draft, Validation, Supervision, Project administration, Methodology, Investigation, Conceptualization.

Declaration of competing interest

The authors declare that they have no known competing financial interests or personal relationships that could have appeared to influence the work reported in this paper.

Data availability

Data will be made available on request.

Acknowledgments

The authors would like to acknowledge Iman Bayat, affiliated with the Ferdowsi University of Mashhad, for his comments and suggestions that greatly improved the manuscript. The authors also would like to thank the editor and anonymous reviewers for the valuable comments.

Appendix A

A.1. Design of the grid

Preliminary analysis using an unstructured mesh has shown that simulations were prone to numerical errors with a non-dissipative central scheme required for LES. Then, as the geometry is simple, a structured mesh is used to keep the solution stable with a pure central scheme (recommended for LES). A no-slip boundary condition on the partition would need a wall-normal grid refinement ($y^+ < 1$) so that, consequently, using a structured mesh, an anisotropic mesh would be generated in the middle of the doorway (with the smallest grid size in the direction of the flow in the doorway and the largest grid size perpendicular to the flow direction). To solve the mixing layer, it is better to limit the mesh anisotropy. This is also better for the definition of the mesh size in the WALE model (i.e., $\sqrt[3]{\bar{V}}$). In addition, the flow is by definition driven by the difference in hydrostatic pressure in both rooms connected by the open door. Therefore, a no-slip condition on the partition wall is expected to have a limited influence on the flow in the doorway.

A.2. Grid size and LES resolution

The grid convergence analysis is not straightforward for LES since, upon further refinement of the LES grid, finer and finer scales are resolved until the LES converges to the DNS. Moreover, the computational cost of a finer grid can be restrictive [41]. However, there are specific criteria to estimate the resolution of a LES [44], such as; the ratio between modeled turbulent viscosity and laminar viscosity, i.e., $\langle \nu_t \rangle / \nu$, the ratio between modeled and total shear stress, the ratio between modeled and total turbulent kinetic energy, and the ratio of integral length scale to cell size.

In this study, the LES resolution is evaluated using three different approaches;

- The resolution of the shear layer between both the warm and cold airstreams is compared to the literature.
- The turbulent kinetic energy ratio is evaluated in the computational domain to check if the LES is sufficiently resolved or not.
- The results of LES for the isothermal case, including discharge coefficient (C_d), temperature and velocity profiles, are compared on a coarse, medium and fine grid containing 31,825,152 cells, 63,203,392 cells and 127,316,480 cells, respectively.

a) The resolution of the shear layer between both the warm and cold airstreams

It is important to capture the flow physics of the shear layer between the counter-flowing airstreams correctly as it directly influences two main phenomena analyzed in our study, meaning the mixing between both airstreams and the flow re-entrainment. It is tricky to assess the resolution of this shear layer using the analysis of the kinetic energy spectrum due to the lack of homogeneous directions in the flow field. Therefore, the resolution can be discussed by comparing the mesh size with other LES of shear layers found in the literature. The maximum time-averaged velocity difference through the shear layer (ΔU) computed using the isothermal case is about 0.4 m/s . The analysis of the velocity profile through the shear layer gives a momentum thickness (θ) and a vorticity thickness (δ) of 0.05 m and 0.18 m , respectively. These values correspond to a Reynolds number based on momentum thickness (Re_θ) of about 1400 and a Reynolds number based on vorticity thickness (Re_δ) of 4800. Close to the doorway, the mesh is almost isotropic with a size (h) of 0.6 cm .

Firstly, Balaras et al. [45] performed LES of a temporally evolving mixing layer from an initial Re_θ of 900 until a Re_θ of 3400. They performed a sensitivity analysis on the domain and grid size to be able to reproduce the flow statistics of DNS data. This study is thus a good reference for comparison. They show that they can reproduce the velocity statistics with a mesh size of 0.85θ , 0.43θ and 0.85θ in streamwise, spanwise and normal directions, respectively. The mesh size in our LES is significantly smaller than these values. Secondly, Pham et al. [46] analyzed the temporal evolution of a stratified shear layer using LES. They investigated the case of a fine LES for an initial Re_δ of 5000. They use a mesh of 0.12δ , 0.12δ and 0.03δ in the streamwise, spanwise and normal directions, respectively. This grid resolution is comparable to our mesh. For instance, their mesh size in the normal direction corresponds to 0.54 cm . Based on these two studies, it can be concluded that the mesh size in our simulation is appropriate to capture the shear layer using LES.

b) The turbulent kinetic energy ratio

Pope [47] recommends the turbulent kinetic energy ratio ($M(x, t)$) as a simple indicator of turbulence resolution. It is defined as the ratio of the unresolved turbulent kinetic energy to the total turbulent kinetic energy:

$$M(x, t) \equiv \frac{k_r(x, t)}{K(x, t) + k_r(x, t)} \quad (23)$$

where $K(x, t)$ and $k_r(x, t)$ indicate the turbulent kinetic energy of the resolved and residual motions, respectively. Smaller values of M correspond to more turbulent motions resolved on the mesh. The limit of $M = 0$ corresponds to DNS while $M = 1$ is representative for a RANS. Based on his suggestion, the turbulence is well resolved by the LES if $M < 0.2$.

Since the turbulent kinetic energy ratio (M) is smaller than 0.09 for LES of thermally stratified rooms, the grid employed for LES is fine enough to simulate the turbulent structures precisely.

c) Comparison of LES results on three different grid resolutions

A grid-sensitivity analysis is conducted for the LES for the case of two isothermal interconnected rooms at different temperatures. The coarse, medium and fine grid contain 31,825,152 cells, 63,203,392 cells and 127,316,480 cells, respectively. The mean streamwise velocity and temperature profiles for three different meshes are plotted along a vertical line in the middle of the doorway in Fig. 10. All three grids provide almost the same profiles, while the fine grid indicates a slight departure from the results of the coarse and medium grids between $0.95 < z < 1.1$. The maximum difference between the coarse and the fine grid in this area goes up to 0.053 m/s and 0.49°C for velocity and temperature, respectively. The shear layer thickness is roughly the same for the three grid resolutions.

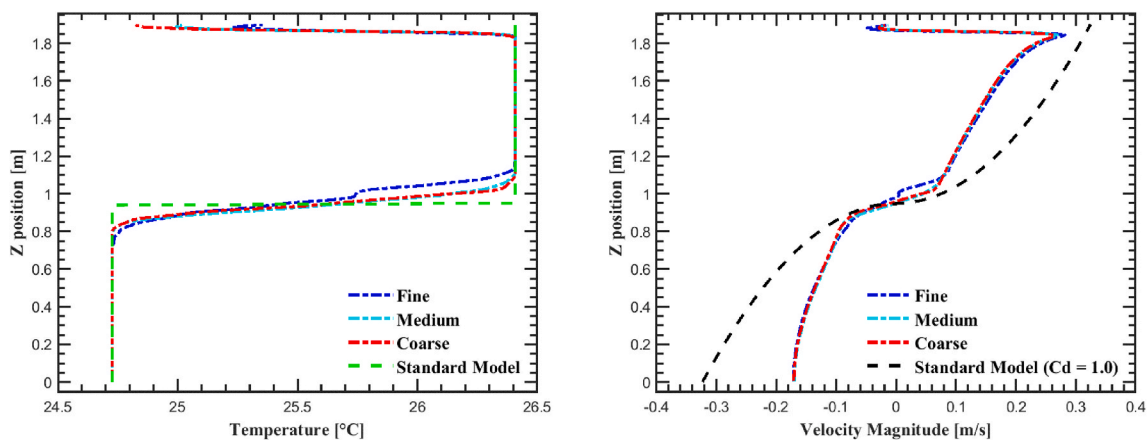






Fig. 10. Time-averaged temperature and streamwise velocity profiles along a vertical line in the middle of the doorway in isothermal rooms on three different grids using LES.

The discharge coefficients, $C_{d,M}$ and $C_{d,Q}$ based on mass (\dot{m}) and heat flows (\dot{Q}) are obtained for the coarse, medium and fine mesh. The data are reported in Table 3.

Table 3

Discharge coefficients obtained based on the mass ($C_{d,M}$) and heat flow rate ($C_{d,Q}$) from LES on three different grids.

		Doorway Plane 		$C_{d,M}$	$C_{d,Q}$
				$C_{d,M} = \frac{\dot{m}_{actual}}{\dot{m}_{max}}$	$C_{d,Q} = \frac{\dot{Q}_{actual}}{\dot{Q}_{max}}$
Isothermal rooms	\dot{m}_{max} and \dot{Q}_{max} based on the averaged room temperature	Coarse Grid		0.511	0.486
		Medium Grid		0.510	0.484
		Fine Grid		0.543	0.506

While the previous two arguments showed that the fine grid was refined enough, the sensitivity analysis on the C_d shows that a coarser grid would not be able to capture the physics properly. The C_d is relatively constant between the coarse and medium meshes but increases significantly for the fine grid.

References

- [1] F. Bazdidi-Tehrani, S. Masoumi-Verki, P. Gholamalipour, Impact of opening shape on airflow and pollutant dispersion in a wind-driven cross-ventilated model building: large eddy simulation, *Sustain. Cities Soc.* 61 (2020), 102196.
- [2] P. Kalliomäki, P. Saarinen, J.W. Tang, H. Koskela, Airflow patterns through single hinged and sliding doors in hospital isolation rooms—Effect of ventilation, flow differential and passage, *Build. Environ.* 107 (2016) 154–168.
- [3] A. Bediako-Bowan, K. Møllbak, J. Kurtzhals, E. Owusu, S. Debrah, M. Newman, Risk factors for surgical site infections in abdominal surgeries in Ghana: emphasis on the impact of operating rooms door openings, *Epidemiol. Infect.* 148 (2020).
- [4] B. Ljungqvist, B. Reinmüller, J. Gustén, L. Gustén, J. Nordenadler, Contamination risks due to door openings in operating rooms, in: 41 St R 3-Nordic Symposium, 2010, p. 148.
- [5] P.E. Saarinen, P. Kalliomäki, J.W. Tang, H. Koskela, Large eddy simulation of air escape through a hospital isolation room single hinged doorway—validation by using tracer gases and simulated smoke videos, *PLoS One* 10 (7) (2015), e0130667.
- [6] X. Shao, K. Hashimoto, L. Fang, A.K. Melikov, K.G. Naydenov, C. Rasmussen, Experimental study of airborne particle transmission through the doorway of a cleanroom due to the movement of a person, *Build. Environ.* 183 (2020), 107205.
- [7] D.W. Etheridge, M. Sandberg, *Building Ventilation: Theory and Measurement*, John Wiley & Sons, Chichester, UK, 1996.
- [8] F. Allard, D. Bienfait, F. Haghghat, G. Liébecq, K. Maas, R. Pelletret, L. Vandaele, Airflow through Large Openings in Buildings, Annex 20: Air Flow Patterns within Buildings, 1992.
- [9] D. Scott, R. Anderson, R. Figliola, Blockage of natural convection boundary layer flow in a multizone enclosure, *Int. J. Heat Fluid Flow* 9 (2) (1988) 208–214.
- [10] J. Neymark, C.R. Boardman III, A. Kirkpatrick, R. Anderson, High Rayleigh number natural convection in partially divided air and water filled enclosures, *Int. J. Heat Mass Tran.* 32 (9) (1989) 1671–1679.
- [11] L. Georges, G. Cao, H.M. Mathisen, Further investigation of the convective heat transfer between rooms through open doorways, in: The 12th REHVA World Congress, vol. 5, Aalborg University, Department of Civil Engineering., Aalborg, 2016.
- [12] E.S. AB, IDA Indoor climate and energy. <http://www.equa.se/en/ida-ice/>, 2013. (Accessed 24 December 2015).
- [13] A. Haas, A. Weber, V. Dorer, W. Keilholz, R. Pelletret, COMIS v3. 1 simulation environment for multizone air flow and pollutant transport modelling, *Energy Build.* 34 (9) (2002) 873–882.
- [14] M.J. Alonso, W.S. Dols, H. Mathisen, Using Co-simulation between EnergyPlus and CONTAM to evaluate recirculation-based, demand-controlled ventilation strategies in an office building, *Build. Environ.* (2021), 108737.
- [15] Q. Chen, Ventilation performance prediction for buildings: a method overview and recent applications, *Build. Environ.* 44 (4) (2009) 848–858.
- [16] F. Allard, Y. Utsumi, Airflow through large openings, *Energy Build.* 18 (2) (1992) 133–145.
- [17] P.K. Heiselberg, L. Jepsen, A. Hylgaard, P.V. Nielsen, M. Perino, Short-Term Airing by Single-Sided Natural Ventilation: Part 1: Measurement of Transient Air Flow Rates, Short-Term Airing by Single-Sided Natural Ventilation, Tsinghua University, 2003, pp. 117–124.
- [18] A. Lefaue, J. Partridge, P. Linden, Regime transitions and energetics of sustained stratified shear flows, *J. Fluid Mech.* 875 (2019) 657–698.
- [19] D. Wilson, D. Kiel, Gravity driven counterflow through an open door in a sealed room, *Build. Environ.* 25 (4) (1990) 379–388.
- [20] W. Brown, K. Solvason, Natural convection through rectangular openings in partitions—1: vertical partitions, *Int. J. Heat Mass Tran.* 5 (9) (1962) 859–868.
- [21] W. Brown, Natural convection through rectangular openings in partitions—2: horizontal partitions, *Int. J. Heat Mass Tran.* 5 (9) (1962) 869–881.
- [22] M. Nansteel, R. Greif, An investigation of natural convection in enclosures with two-and three-dimensional partitions, *Int. J. Heat Mass Tran.* 27 (4) (1984) 561–571.
- [23] M. Nansteel, R. Greif, *Natural Convection in Undivided and Partially Divided Rectangular Enclosures*, 1981.
- [24] P. Favaro, H. Manz, Temperature-driven single-sided ventilation through a large rectangular opening, *Build. Environ.* 40 (5) (2005) 689–699.
- [25] D. Agonafer, L. Gan-Li, D.B. Spalding, The LVEL turbulence model for conjugate heat transfer at low Reynolds numbers, Application of CAE/CAD Electronic Systems, *ASME* 18 (1996) 23–26.
- [26] W. Zhang, Q. Chen, Large eddy simulation of indoor airflow with a filtered dynamic subgrid scale model, *Int. J. Heat Mass Tran.* 43 (17) (2000) 3219–3231.
- [27] Y. Jiang, Q. Chen, Study of particle dispersion in buildings with large eddy simulation, *Proceedings of Indoor Air 2* (2002).
- [28] N. Ivanov, M. Zaslomova, Large eddy simulation of airflow in a room with a sidewall jet: comparison with benchmark test data for occupied zone, in: *Proc. of Roomvent & Ventilation 2018: Excellent Indoor Climate and High Performing Ventilation*, 2018, pp. 319–324.
- [29] B. Blocken, LES over RANS in Building Simulation for Outdoor and Indoor Applications: a Foregone Conclusion?, *Building Simulation*, Springer, 2018, pp. 821–870.
- [30] Z. Zhang, W. Zhang, Z.J. Zhai, Q.Y. Chen, Evaluation of various turbulence models in predicting airflow and turbulence in enclosed environments by CFD: Part 2—comparison with experimental data from literature, *HVAC R Res.* 13 (6) (2007) 871–886.
- [31] W.K. Chow, G. Zou, Correlation equations on fire-induced air flow rates through doorway derived by large eddy simulation, *Build. Environ.* 40 (7) (2005) 897–906.
- [32] J.D. Balcomb, *Heat Distribution by Natural Convection*, Intersol Eighty Five, Elsevier 1986, pp. 277–281.
- [33] D.D. Weber, *Similitude Modeling of Natural Convection Heat Transfer through an Aperture in Passive Solar Heated Buildings*, 1981.
- [34] R. Pelletret, H. Khodr, E. de Sophia Antipolis, A New Model to Compute Air Distribution, *Building Simulation*, 1989, pp. 291–296.
- [35] P. Minard, Experimental Study of the Temperature and Velocity Distribution through a Doorway between a Warm and a Cold Room, Norwegian University of Science and Technology, 2015.
- [36] F. Nicoud, F. Ducros, Subgrid-scale stress modelling based on the square of the velocity gradient tensor, *Flow, Turbul. Combust.* 62 (3) (1999) 183–200.
- [37] A. Leonard, Energy cascade in large-eddy simulations of turbulent fluid flows, *Adv. Geophys.* 18 (A) (1974) 237–248.
- [38] F. Piscaglia, A. Montorfano, A. Onorati, F. Brusiani, Boundary conditions and sgs models for les of wall-bounded separated flows: an application to engine-like geometries, *Oil Gas Sci. Technol. Revue d'IFP Energies nouvelles* 69 (1) (2014) 11–27.
- [39] A. Yuen, G. Yeoh, V. Timchenko, S. Cheung, T. Chen, Study of three LES subgrid-scale turbulence models for predictions of heat and mass transfer in large-scale

- compartment fires, *Numer. Heat Tran., Part A: Applications* 69 (11) (2016) 1223–1241.
- [40] F. Bazdidi-Tehrani, S. Masoumi-Verki, P. Gholamalipour, M. Kiamansouri, Large Eddy Simulation of Pollutant Dispersion in a Naturally Cross-Ventilated Model Building: Comparison between Sub-grid Scale Models, *Building Simulation*, Springer, 2019, pp. 921–941.
- [41] N. Arya, A. De, Effect of grid sensitivity on the performance of wall adapting SGS models for LES of swirling and separating–reattaching flows, *Comput. Math. Appl.* 78 (6) (2019) 2035–2051.
- [42] V. Yakhot, S.A. Orszag, Renormalization group analysis of turbulence. I. Basic theory, *J. Sci. Comput.* 1 (1) (1986) 3–51.
- [43] J.L. Hensen, R. Lamberts, *Building Performance Simulation for Design and Operation*, Routledge, 2012.
- [44] L. Davidson, *Fluid Mechanics, Turbulent Flow and Turbulence Modeling*, Chalmers University of Technology, Goteborg, Sweden, 2018. Nov 2011.
- [45] E. Balaras, U. Piomelli, J.M. Wallace, Self-similar states in turbulent mixing layers, *J. Fluid Mech.* 446 (2001) 1–24.
- [46] H.T. Pham, S. Sarkar, Large eddy simulations of a stratified shear layer, *J. Fluid Eng.* 136 (6) (2014).
- [47] S.B. Pope, Ten questions concerning the large-eddy simulation of turbulent flows, *New J. Phys.* 6 (1) (2004) 35.